Porosity and grain size controls on compaction band formation in Jurassic Navajo Sandstone

Richard A. Schultz,[1] Chris H. Okubo,[2] and Haakon Fossen[3,4]

Received 28 July 2010; revised 5 October 2010; accepted 8 October 2010; published 20 November 2010.

[1] Determining the rock properties that permit or impede the growth of compaction bands in sedimentary sequences is a critical problem of importance to studies of strain localization and characterization of subsurface geologic reservoirs. We determine the porosity and average grain size of a sequence of stratigraphic layers of Navajo Sandstone that are then used in a critical state model to infer plastic yield envelopes for the layers. Pure compaction bands are formed in layers having the largest average grain sizes (0.42–0.45 mm) and porosities (28%), and correspondingly the smallest values of critical pressure (~22 MPa) in the sequence. The results suggest that compaction bands formed in these layers after burial to ~1.5 km depth in association with thrust faulting beneath the nearby East Kaibab monocline, and that hardening of the yield caps accompanied compactional deformation of the layers. **Citation:** Schultz, R. A., C. H. Okubo, and H. Fossen (2010), Porosity and grain size controls on compaction band formation in Jurassic Navajo Sandstone, *Geophys. Res. Lett.*, *37*, L22306, doi:10.1029/2010GL044909.

1. Introduction

[2] The productivity for petroleum and groundwater, and CO_2 sequestration potential, of subsurface geologic reservoirs is in part affected by the spatial distribution of structural discontinuities such as fractures and deformation bands. Compaction bands are a type of deformation band characterized by a reduction in porosity and permeability across a tabular zone, in which compactional strains equal or exceed shear strains, that is typically a few mm's to cm's thick [e.g., *Fossen et al.*, 2007]. Compaction bands are only found in medium to coarse-grained sandstone layers of very high porosity and are so far only reported from a few localities in the world [e.g., *Mollema and Antonellini*, 1996; *Sternlof et al.*, 2005; *Holcomb et al.*, 2007]. Understanding the controls on compaction band formation is of great interest because these tabular zones of reduced permeability could act as baffles to subsurface fluid flow.

[3] Laboratory experiments and theoretical work suggest that compaction bands may form under particular sets of evolving host-rock properties, stress states, and loading paths [e.g., *Olsson*, 1999, 2000; *Issen and Rudnicki*, 2000; *Bésuelle and Rudnicki*, 2004], and field relations demonstrate that compaction bands can be restricted to certain layers within the same stratigraphic unit [e.g., *Mollema and Antonellini*, 1996; *Eichhubl et al.*, 2010]. A key question is what petrophysical properties permit, or impede, the growth of compaction bands under a particular stress state [e.g., *Olsson*, 1999; *Wong et al.*, 2001; *Haimson and Lee*, 2004; *Stanchits et al.*, 2009]. Such alternating compaction band-rich and compaction band-free layers are often sufficiently thin (a few 10's of cm) that they can be assumed to have undergone the same overall deformation histories. The selective formation of compaction bands in such sequences indicates that strain was accommodated differently in adjacent layers. In this paper we explore why this is the case.

[4] We address this question by analyzing a remarkable outcrop of compaction bands in south central Utah. The compaction band locality studied by *Mollema and Antonellini* [1996] and *Schultz* [2009] contains an outcrop of Jurassic Navajo Sandstone where several sets of compaction bands are well exposed in cross-section (Figure 1). Using field and microstructural observations from this exposure, we investigate the effects that porosity and grain size had in facilitating or impeding the growth of compaction bands under a particular stress state.

2. Description of the Field Locality

[5] The field locality is adjacent to the East Kaibab monocline in south central Utah. The monocline trends north–northeast and is approximately 250 km long. Growth of the East Kaibab monocline is attributed to oblique-thrust reactivation of Proterozoic normal faults during the Laramide [e.g., *Tindall and Davis*, 1999; *Bump and Davis*, 2003]. Permian- to Cretaceous-aged sedimentary rocks are exposed along the monocline in this area [*Sargent and Hansen*, 1982]. The major causative reverse faults of the monocline lie approximately 2.5 km to the west of the field locality, where total displacement across the east-facing monocline and its associated reverse faults is about 1500 m [*Doelling and Willis*, 2006]. Strata at the field locality dip at less than ~10° toward the east.

[6] The Jurassic Navajo Sandstone exposed at the field locality contains a sequence of five adjacent sandstone layers of different characteristics and origin (Table 1). Layer 1 is a massive sand unit formed by soft-sediment deformation shortly after deposition, defining what is classified as reworked structureless sandstone by *Chan et al.* [2007]. The underlying layers 2–4 are part of a dune sequence, where layers 2 and 4 represent grain-flow dune units and layer 3 is a grain-fall unit. The lower layer (layer 5) is a relatively fine-grained and less well-sorted sandstone, interpreted here as a wind ripple layer located at the toe of the dune.

[1] Geomechanics–Rock Fracture Group, Department of Geological Sciences and Engineering, University of Nevada, Reno, Nevada, USA.
[2] U.S. Geological Survey, Flagstaff, Arizona, USA.
[3] Department of Earth Science, University of Bergen, Bergen, Norway.
[4] CIPR, Bergen, Norway.

0094-8276/10/2010GL044909

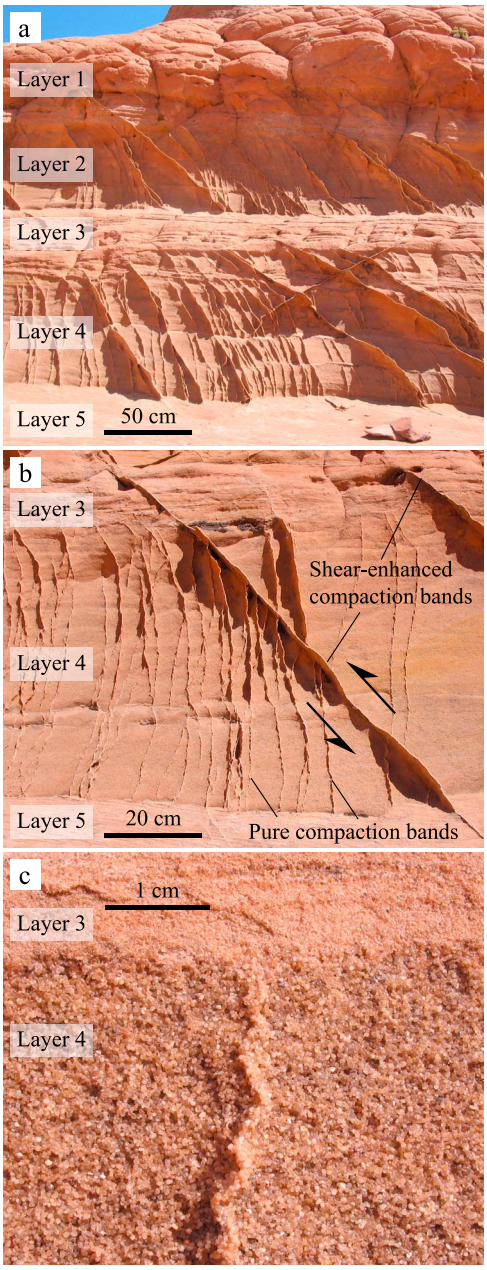

Figure 1. Compaction bands in the field locality in south central Utah (37.0526°N, −111.9859°W). (a) Outcropping of the five sandstone layers analyzed in this study and the attendant compaction bands. (b) Example of the near-vertical, pure compaction bands and the dipping, shear-enhanced compaction bands. (c) Termination of a pure compaction band along the contact between layers 3 and 4.

[7] Two types of compaction bands are observed in the sequence. The first set is characterized by thin mm-thick vertical bands with a wiggly geometry that are confined to grain-flow layers 2 and 4, where they are abundant (Figure 1). These bands show compaction but little if any evidence in thin sections of shear displacement at the grain scale and correspond to the "crooked" compaction bands of *Mollema and Antonellini* [1996]. The other set consists of steeply dipping bands that also occur in layers 2 and 4, some of which extend into layer 3. These bands differ from pure compaction bands, being quasi-planar and up to several cm thick with compaction along with small shearing offsets discernible in thin section and where they offset pre-existing markers such as fine-scale eolian crossbeds. This second set of bands is interpreted in this paper as shear-enhanced compaction bands [*Eichhubl et al.*, 2010] in which compactional and shearing strains are comparable in magnitude, with offsets on the order of a few mm or less. Bedding crosscut by these bands has a reverse sense of offset.

[8] Field relations show that both sets of compaction bands formed contemporaneously. Some of the pure compaction bands in layers 2 and 4 transition to shear-enhanced compaction bands in layer 3. Such bands are continuous across the layer interfaces, but show a change in morphology, orientation, and strain. These bands are near-vertical in layers 2 and 4, similar to the pure compaction bands in these layers, but dip at approximately 50°–60° toward the east in layer 3, consistent with other shear-enhanced compaction bands in this layer. The bands are wiggly with small or negligible shear offsets in layers 2 and 4 yet become quasi-planar and show unambiguous shear offsets of bedding in layer 3. Some bands also transition between shear-enhanced compaction and pure compaction bands in layers 2 and 4.

[9] The orientations and sense of strain across the compaction bands are also consistent with the formation of both band types under the same remote stress field. Assuming that the pure compaction bands are oriented with their normal vectors at ~0° to the direction of maximum remote compressive principal stress σ_1, the shear-enhanced compaction bands would be oriented with normal vectors at 30–40° to σ_1. This stress orientation would account for the observed reverse sense of shearing offset, plus band-normal compactional strain, along the shear-enhanced compaction bands. The angular relations for shear-enhanced compaction bands noted here are consistent with those identified for compactional/shear deformation bands in the field [*Eichhubl et al.*, 2010], experiment, [e.g., *Olsson*, 1999, 2000; *Wong et al.*, 2001], and theory [e.g., *Bésuelle and Rudnicki*, 2004; *Rudnicki*, 2004].

[10] Shear bands with no evidence of grain crushing, known as disaggregation bands in much of the literature [*Fossen et al.*, 2007] occur in layers 3 and 5. The bands locally extend into layers 2 and 4 and are mm's to a cm thick. These bands dip at approximately 70° to near vertical toward the northwest and exhibit a normal sense of displacement. Crosscutting relationships clearly show that these disaggregation bands predate the pure compaction and shear-enhanced compaction bands. For instance, pure compaction bands terminate (but are not offset) at their intersection with these bands, and shear enhanced compac-

Table 1. Properties of the Layers

Layer	Facies	Average Porosity[a]	Average Grain Size[a] (mm)	P^* [b] (MPa)
1	Sand injectite	0.17 ± 0.034	0.16 ± 0.013	222.9 ± 16.8
2	Grain flow unit	0.28 ± 0.0032	0.42 ± 0.071	24.8 ± 1.9
3	Grain fall unit	0.24 ± 0.019	0.27 ± 0.011	60.6 ± 4.6
4	Grain flow unit	0.28 ± 0.012	0.45 ± 0.025	22.4 ± 1.7
5	Wind ripple unit	0.17 ± 0.012	0.21 ± 0.092	148.3 ± 7.7

[a]Uncertainties are ±1σ.
[b]Range for 5% uncertainty in porosity values.

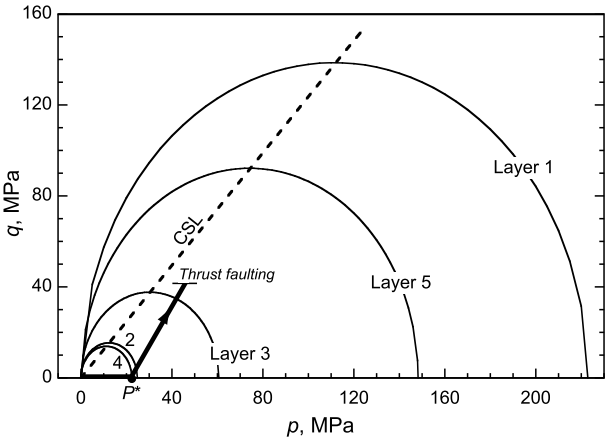

Figure 2. Plastic yield envelopes for all five layers plotted on the q-p diagram. Solid line with arrow shows possible loading path (see text for discussion).

tion bands show reverse offsets of crosscut pure compaction and disaggregation bands.

3. Background and Methods

[11] The deformational characteristics of porous soils and sedimentary rocks are captured by plastic yield envelopes that close at high confining pressure, leading to dilatant frictional behavior at lower confining pressures and compactional, strain-hardening behavior at higher pressures [e.g. *Zhang et al.*, 1990; *Wong et al.*, 1992, 2004; *Cuss et al.*, 2003; *Lade*, 2005; *Wibberley et al.*, 2007]. The closure of these yield envelopes at higher confining pressures results from shear-induced compaction, strain-hardening, and macroscopic flow [e.g., *Muir Wood*, 1990; *Davis and Selvadurai*, 2002; *Aydin et al.*, 2006]. The yield envelopes are presented on a q-p diagram with axes

$$q = (\sigma_1 - \sigma_3)$$
$$p = \frac{(\sigma_1 + \sigma_2 + \sigma_3)}{3} \quad (1)$$

in which σ_1, σ_2, and σ_3 are the principal effective stresses (compression positive, with $\sigma_1 > \sigma_2 > \sigma_3$), so that q is differential stress and p is confining pressure. To first order, the shape of the plastic yield envelope for a porous granular solid such as a sandstone has an elliptical form in the compactional regime, called a cap [e.g., *Wong et al.*, 1992]. The equation of the yield envelope is given by [*Davis and Selvadurai*, 2002, p. 71]

$$q^2 = M^2 p(P^* - p) \quad (2)$$

in which the slope of the critical-state line, representing the boundary between dilatant and compactional behavior, is given by $M = (6\sin\phi)/(3 - \sin\phi)$, ϕ is the angle of friction of the host rock, and P^* is the critical pressure (in MPa) for the onset of pore collapse and grain breakage, which is given approximately by $P^* = (nR)^{-1.5}$ [*Zhang et al.*, 1990] in which n is the porosity (expressed as fractional, not as percent) and R is the average grain size (in mm) of host rock. Because the onset of shear-enhanced compaction in porous granular rocks scales with the plastic yield strength P^* [*Wong and Baud*, 1999; *Wong et al.*, 2004], we use this parameter as a measure of the relative compactional strengths of each layer in the studied outcrop.

[12] The grain-size analysis for each of the five layers was accomplished by choosing representative images of thin sections of the host rock (see auxiliary material) and measuring all grains intersected by one or two lines drawn diagonally across the layering [e.g., *Zhang et al.*, 1990].[1] Porosity and average grain size were obtained from averaging measurements made from four thin sections for layer 1, two from layer 2, three from layer 3, two from layer 4, and three from layer 5. The average grain-size value was used in the calculation of layer yield strength, rather than maximum grain size, consistent with previous work that demonstrates a good correspondence between P^* calculated using average grain size and independent determination of the critical pressure in triaxial laboratory tests [*Zhang et al.*, 1990]. Porosity was measured digitally by manually converting the same thin section images into binary images, separating epoxy-filled pore area from grains.

4. Results and Discussion

[13] Measurements of porosity and grain size for each layer are listed in Table 1. The largest porosity, 28%, and largest average grain size, 0.42–0.45 mm, are found for layers 2 and 4, respectively, both of which contain pure compaction bands. Thick, shear-enhanced compaction bands are found in layers 2, 3, and 4, with layer 3 having n = 24% and R = 0.27 mm. The upper and lower layers (1 and 5) have the smallest values of porosity and grain size of the sequence. Consequently, the critical pressures P^*, and therefore the plastic yield envelopes, are smallest for layers 2 and 4 and largest for layers 1 and 5 (Figure 2). The value of P^* for layers 2 and 4, 22–25 MPa, is consistent with that reported for unconsolidated sands by *Wong and Baud* [1999].

[14] Post-band compaction probably occurred to a minor extent through grain contact dissolution. Dissolution at grain contacts has occurred, but the amount of dissolution is not very large. Our thin sections also reveal little if any cementation in the host rock. We infer that the reduction in porosity in the host sandstone during burial and/or deformation was small, perhaps on the order of a few percent. To estimate the potential variability in P^* with porosity, we calculated P^* for porosity values varying within 5% of those measured (see Table 1). The resulting uncertainty in P^* was less than ±2 MPa for layers 2 and 4 that host pure compaction bands, and somewhat more for other layers.

[15] The stress states for band formation may be estimated from the plastic yield envelopes. Building on work by *Anderson* [1951], *McGarr* [1988] concluded that the stress state within a sedimentary layer undergoing burial and lithification would be given approximately by a lithostatic state of stress; i.e., $\sigma_1 = \sigma_2 = \sigma_3 = \sigma_v = \rho g z$, with σ_v being the vertical effective principal stress, ρ the average rock density assuming hydrostatic pore-water pressure, and z the depth. This initial stress state was also favored by *Jaeger*

[1] Auxiliary materials are available in the HTML. doi:10.1029/2010GL044909.

et al. [2007, p. 400–401] over $\sigma_h = [\nu/(1-\nu)]\sigma_v$, where ν is Poisson's ratio, which assumes zero lateral strain and an absence of gravitational body forces, and thus represents an extreme, if not unrealistic, situation in the crust. The loading path for burial would then plot as a horizontal line on the q-p diagram (heavy line on Figure 2 along $q = 0$ between $0 \le p < P^*$), similar conceptually to the sub-horizontal "near isotropic burial" curve of *Saillet and Wibberley* [2010].

[16] Pure compaction bands in layers 2 and 4 imply that the stress state in the layer before the time of band formation was approximately lithostatic. Using the second expression of equation (1), $P^* = \sigma_v$. Using values of $P^* = 22$ MPa (Table 1), $g = 9.8$ m/s^2, an average dry-rock density $\rho = 2{,}450$ kg/m^3 and hydrostatic pore-fluid conditions, $z = 1.5$ km before the time of band formation. This estimate of paleo-depth is consistent with the approximate depth of burial, 0.9–1.7 km, estimated independently from stratigraphic constraints [*Schultz*, 2009]. Formation of pure compaction bands on an elliptic yield cap for values of $p < P^*$ (and therefore, $q \neq 0$) is indicated by theoretical and experimental results [e.g., *Rudnicki*, 2004; *Grueschow and Rudnicki*, 2005]. Vertical compaction bands in layers 2 and 4 require that σ_1 be horizontal and larger than σ_v, implying that the depth estimate is a maximum value.

[17] Previous work suggests that the rocks in the field locality were deformed in a thrust-faulting tectonic environment near the East Kaibab monocline [e.g., *Mollema and Antonellini*, 1996; *Schultz*, 2009; *Solum et al.*, 2010], perhaps above the blind tip of a reactivated reverse fault [*Schultz*, 2010], with $\sigma_1 > \sigma_2 \sim \sigma_3 = \sigma_v$, following *Bésuelle and Rudnicki* [2004] and *Issen and Challa* [2008]. A thrust-faulting regional stress state is given approximately by $\sigma_1/\sigma_3 = k$, where $\sigma_1 = \sigma_H$, $\sigma_3 = \sigma_v$, and k is a parameter related to the average friction coefficient of the host rock, given by $k = \left(\sqrt{\mu^2+1}+\mu\right)^2$. Typical friction angles for sandstones are in the range of 30° [e.g., *Paterson and Wong*, 2005], corresponding to $k = 3.1$. A plausible loading path leading from the burial-related lithostat to thrust faulting is shown in Figure 2. The loading path was calculated by holding σ_v constant and incrementing σ_1 with $\sigma_2 = \sigma_3$. Layer 3 is intersected by the loading path below the critical state line (CSL in Figure 2), indicating compactional and shear strains for bands in that layer, consistent with field observations. The loading path is applicable for $p < 46$ MPa, as this point corresponds to $\sigma_1/\sigma_3 < 3.1$; greater values of q and p would correspond to a change in deformation mechanism in the host rock, from banding to frictional sliding. This analysis suggests that shear-enhanced compaction bands in layer 3 grew before the thrust faulting stress state was achieved, whereas the yield strengths of layers 5 and 1 were sufficiently large for deformation banding not to have occurred in those layers.

[18] Analyses of localization conditions for bands on an elliptic yield cap suggest that bands with compaction and shear can form at small angles to σ_1 (i.e., with normal vectors oriented <45° to σ_1), as we observe in layers 2 and 4. Shear-enhanced compaction bands in these layers have orientations (30–40°) that are consistent with, if somewhat larger than, those calculated by *Rudnicki* [2004] (i.e., <35° to σ_1). Increases in band angle relative to σ_1 can occur for yield caps having a different shape than those assumed in equation (2). For example, non-isotropic hardening [see *Grueschow and Rudnicki*, 2005, Figure 5] that produces a cap with the maximum value of $q < P^*/2$ (leading to an increased cap ellipticity and decreased value of normalized confining stress S [*Rudnicki*, 2004]) predicts larger band angles, as do non-associated flow rules on the cap. We hypothesize that the growth of pure compaction bands in layers 2 and 4 contributed to volumetric decreases and plastic hardening in these layers that led to sufficient non-isotropic cap hardening, and/or departure from normality, for shear-enhanced compaction bands to have formed at angles of 30–40° to σ_1.

5. Conclusions

[19] Using a sequence of layers within Navajo Sandstone we identify the values of porosity and average grain size of layers that host pure and shear-enhanced compaction bands, and of layers that don't. The corresponding plastic yield envelopes are smallest for layers having the largest values of porosity and average grain size in the sequence, and largest for finer-grained, less porous layers that lack compaction bands. The development of pure compaction bands in the sequence implies compaction accompanying burial to depths of ~1.5 km, followed by a loading path that promoted the growth of compaction bands having a combination of shearing and compactional deformation in the most porous layers. This work sets the framework for inferring compaction-band deformation elsewhere by identifying combinations of stress state and layer properties favorable to this class of deformation.

[20] **Acknowledgments.** We thank Peter Eichhubl and an anonymous reviewer for their helpful comments. This work was supported by NASA's Planetary Geology and Geophysics Program (grant to RAS) and by NASA's Mars Fundamental Research Program (grant to CHO).

References

Anderson, E. M. (1951), *The Dynamics of Faulting*, 2nd ed., 206 pp., Oliver and Boyd, Edinburgh, U. K.

Aydin, A., R. I. Borja, and P. Eichhubl (2006), Geological and mathematical framework for failure modes in granular rock, *J. Struct. Geol.*, *28*, 83–98, doi:10.1016/j.jsg.2005.07.008.

Bésuelle, P., and J. W. Rudnicki (2004), Localization: Shear bands and compaction bands, in *Mechanics of Fluid-Saturated Rocks*, edited by Y. Guéguen and M. Boutéca, pp. 219–321, Elsevier, Amsterdam.

Bump, A. P., and G. H. Davis (2003), Late Cretaceous-Early Tertiary Laramide deformation of the northern Colorado Plateau, Utah and Colorado, *J. Struct. Geol.*, *25*, 421–440, doi:10.1016/S0191-8141(02)00033-0.

Chan, M. A., D. Netoff, R. C. Blakey, G. Kocurek, and W. Alvarez (2007), Clastic-injection pipes and syndepositional deformation structures in Jurassic eolian deposits: Examples from the Colorado Plateau, in *Sand Injectites: Implications for Hydrocarbon Exploration and Production*, edited by A. Hurst and J. A. Cartwright, *AAPG Mem.*, *87*, 233–244.

Cuss, R. J., E. H. Rutter, and R. F. Holloway (2003), The application of critical state soil mechanics to the mechanical behaviour of porous sandstones, *Int. J. Rock Mech. Min. Sci.*, *40*, 847–862, doi:10.1016/S1365-1609(03)00053-4.

Davis, R. O., and A. P. S. Selvadurai (2002), *Plasticity and Geomechanics*, 287 pp., doi:10.1017/CBO9780511614958, Cambridge Univ. Press, Cambridge, U. K.

Doelling, H. H., and G. C. Willis (2006), Geologic map of the Smoky Mountain 30′ × 60′ quadrangle, Kane and San Juan Counties, Utah, and Coconino County, Arizona, Utah Geol. Surv., Salt Lake City.

Eichhubl, P., J. N. Hooker, and S. E. Laubach (2010), Pure and shear-enhanced compaction bands in Aztec sandstone, *J. Struct. Geol.*, doi:10.1016/j.jsg.2010.02.004, in press.

Fossen, H., R. A. Schultz, Z. K. Shipton, and K. Mair (2007), Deformation bands in sandstone: A review, *J. Geol. Soc.*, *164*, 755–769, doi:10.1144/0016-76492006-036.

Grueschow, E., and J. W. Rudnicki (2005), Elliptic yield cap constitutive modeling for high porosity sandstone, *Int. J. Solids Struct.*, *42*, 4574–4587, doi:10.1016/j.ijsolstr.2005.02.001.

Haimson, B., and H. Lee (2004), Borehole breakouts and compaction bands in two high-porosity sandstones, *Int. J. Rock Mech. Min. Sci.*, *41*, 287–301, doi:10.1016/j.ijrmms.2003.09.001.

Holcomb, D., J. W. Rudnicki, K. A. Issen, and K. Sternlof (2007), Compaction localization in the Earth and the laboratory: State of the research and research directions, *Acta Geotech.*, *2*, 1–15, doi:10.1007/s11440-007-0027-y.

Issen, K. A., and V. Challa (2008), Influence of the intermediate principal stress on the strain localization mode in porous sandstone, *J. Geophys. Res.*, *113*, B02103, doi:10.1029/2005JB004008.

Issen, K. A., and J. W. Rudnicki (2000), Conditions for compaction bands in porous rock, *J. Geophys. Res.*, *105*, 21,529–21,536, doi:10.1029/2000JB900185.

Jaeger, J. C., N. G. W. Cook, and R. W. Zimmermann (2007), *Fundamentals of Rock Mechanics*, 4th ed., 475 pp., Blackwell, Oxford, U. K.

Lade, P. V. (2005), Overview of constitutive models for soils, in *Soil Constitutive Models: Evaluation, Selection, and Calibration*, edited by J. A. Yamamuro and V. N. Kalaikin, pp. 1–34, *ASCE Geotech. Spec. Publ.*, *128*.

McGarr, A. (1988), On the state of lithospheric stress in the absence of applied tectonic forces, *J. Geophys. Res.*, *93*, 13,609–13,617, doi:10.1029/JB093iB11p13609.

Mollema, P. N., and M. A. Antonellini (1996), Compaction bands: A structural analog for anti-mode I cracks in aeolian sandstone, *Tectonophysics*, *267*, 209–228, doi:10.1016/S0040-1951(96)00098-4.

Muir Wood, D. (1990), *Soil Behaviour and Critical State Soil Mechanics*, 462 pp., Cambridge Univ. Press, Cambridge, U. K.

Olsson, W. A. (1999), Theoretical and experimental investigation of compaction bands in porous rock, *J. Geophys. Res.*, *104*, 7219–7228, doi:10.1029/1998JB900120.

Olsson, W. A. (2000), Origin of Lüders' bands in deformed rock, *J. Geophys. Res.*, *105*, 5931–5938, doi:10.1029/1999JB900428.

Paterson, M. S., and T.-F. Wong (2005), *Experimental Rock Deformation—The Brittle Field*, 2nd ed., 347 pp., Springer, Berlin.

Rudnicki, J. W. (2004), Shear and compaction band formation on an elliptic yield cap, *J. Geophys. Res.*, *109*, B03402, doi:10.1029/2003JB002633.

Saillet, E., and C. A. J. Wibberley (2010), Evolution of cataclastic faulting in high-porosity sandstone, Bassin du Sud-Est, Provence, France, *J. Struct. Geol.*, doi:10.1016/j.jsg.2010.02.007, in press.

Sargent, K. A., and S. E. Hansen (1982), Bedrock geologic map of the Kaiparowits coal-basin area, Utah, *U.S. Geol. Surv. Misc. Invest. Map*, *I-1033-I*.

Schultz, R. A. (2009), Scaling and paleodepth of compaction bands, Nevada and Utah, *J. Geophys. Res.*, *114*, B03407, doi:10.1029/2008JB005876.

Schultz, R. A. (2010), Relationship of compaction bands in Utah, USA, to monoclinal folding, *Geophys. Res. Abstr.*, *12*, Abstract EGU/2010-1970.

Solum, J. G., J. P. Brandenburg, O. V. Kostenko, S. J. Wilkins, and R. A. Schultz (2010), Characterization of deformation bands associated with normal and reverse stress states in the Navajo Sandstone, Utah, *AAPG Bull.*, *94*, 1453–1475, doi:10.1306/01051009137.

Stanchits, S., J. Fortin, Y. Gueguen, and G. Dresen (2009), Initiation and propagation of compaction bands in dry and wet Bentheim Sandstone, *Pure Appl. Geophys.*, *166*, 843–868, doi:10.1007/s00024-009-0478-1.

Sternlof, K. R., J. W. Rudnicki, and D. D. Pollard (2005), Anticrack inclusion model for compaction bands in sandstone, *J. Geophys. Res.*, *110*, B11403, doi:10.1029/2005JB003764.

Tindall, S. E., and G. H. Davis (1999), Monocline development by oblique-slip fault-propagation folding: The East Kaibab monocline, Colorado Plateau, Utah, *J. Struct. Geol.*, *21*, 1303–1320, doi:10.1016/S0191-8141(99)00089-9.

Wibberley, C. A. J., J.-P. Petit, and T. Rives (2007), The mechanics of fault distribution and localization in high-porosity sands, Provence, France, in *The Relationship Between Damage and Localization*, edited by H. Lewis and G. D. Couples, *Geol. Soc. London Spec. Publ.*, *289*, 19–46.

Wong, T.-F., and P. Baud (1999), Mechanical compaction of porous sandstone, *Oil Gas Sci. Technol. Rev. Inst. Francais Pet.*, *54*, 715–727.

Wong, T.-F., H. Szeto, and J. Zhang (1992), Effect of loading path and porosity on the failure mode of porous rocks, *Appl. Mech. Rev.*, *45*, 281–293, doi:10.1115/1.3119759.

Wong, T.-F., P. Baud, and E. Klein (2001), Localized failure modes in a compactant porous rock, *Geophys. Res. Lett.*, *28*, 2521–2524, doi:10.1029/2001GL012960.

Wong, T.-F., C. David, and B. Menéndez (2004), Mechanical compaction, in *Mechanics of Fluid-Saturated Rocks*, edited by Y. Guéguen and M. Boutéca, pp. 55–114, Elsevier, Amsterdam.

Zhang, J., T.-F. Wong, and D. M. Davis (1990), Micromechanics of pressure-induced grain crushing in porous rocks, *J. Geophys. Res.*, *95*, 341–352, doi:10.1029/JB095iB01p00341.

H. Fossen, Department of Earth Science, University of Bergen, Allégt. 41, N-5007 Bergen, Norway.

C. H. Okubo, U.S. Geological Survey, 2255 North Gemini Dr., Flagstaff, AZ 86001, USA.

R. A. Schultz, Geomechanics–Rock Fracture Group, Department of Geological Sciences and Engineering, University of Nevada, Reno, NV 89557, USA. (schultz@mines.unr.edu)